



LAWRENCE
LIVERMORE
NATIONAL
LABORATORY

Simulations of 3w Beam Filamentation in the Beamlet Focus Lens and General Comments on Filamentation Theory

M. Spaeth, M. Henesian

September 30, 2014

Disclaimer

This document was prepared as an account of work sponsored by an agency of the United States government. Neither the United States government nor Lawrence Livermore National Security, LLC, nor any of their employees makes any warranty, expressed or implied, or assumes any legal liability or responsibility for the accuracy, completeness, or usefulness of any information, apparatus, product, or process disclosed, or represents that its use would not infringe privately owned rights. Reference herein to any specific commercial product, process, or service by trade name, trademark, manufacturer, or otherwise does not necessarily constitute or imply its endorsement, recommendation, or favoring by the United States government or Lawrence Livermore National Security, LLC. The views and opinions of authors expressed herein do not necessarily state or reflect those of the United States government or Lawrence Livermore National Security, LLC, and shall not be used for advertising or product endorsement purposes.

This work performed under the auspices of the U.S. Department of Energy by Lawrence Livermore National Laboratory under Contract DE-AC52-07NA27344.

***Inertial Confinement Fusion Program
ICF Laser Science and Technology
Laser Modeling and Optimization Group***

Mail Station L-490
Ext. 3-1504

LS&T-LMO-96-001

Date: May 28, 1996

To: Distribution

From: Mark A. Henesian

Subject: Simulations of 3ω Beam Filamentation in the Beamlet Focus Lens
and General Comments on Filamentation Theory[†]

Abstract:

The IL threshold for filamentation at 3ω in the fused silica Beamlet focusing lens is estimated to be greater than or equal to ~ 22 GW/cm with the current refinished crystals, where I is the nominal 3ω intensity at the exit plane of the tripling crystal, and L is the distance into the lens material, providing safe 3ω Beamlet operation up to 4 GW/cm².

This value includes estimated nonlinear refraction effects from the residual 1ω and 2ω light, and changes in modulation from the ~ 10 -cm gap between the doubling and tripling crystals. At the thickest (5-cm) side of the focus lens, we project that Beamlet will be safe from filamentation-induced optical damage provided the crystals have 4-nm or less r.m.s. roughness per surface as measured over 10-mm regions using a Zygo GPIxp interferometer, and have a PSD (power spectral density) typical of the current best crystals. Representative crystal data was used for these simulations, and then scaled upward to estimate the filamentation risk with rougher surface finish. The recently re-finished 37-cm Beamlet doubler and tripler crystals have surfaces that range from 1.2 to 3.2 nm r.m.s. roughness as measured with the Zygo GPIxp and appear to meet this specification.¹ We haven't attempted to include any effects from small obscurations or damage spots on the KDP crystals or the focus lens.

[†] submitted as part of the package of materials for the NIF Technical Lecture Series presented to the Second Annual International Conference on Solid State Lasers for Application to Inertial Confinement Fusion (ICF), October 22 through 25, 1996, Paris, France.

The calculations presented here lead to a more conservative estimate of the filamentation damage threat on Beamlet than recent simulations of OSL filamentation experiments,² since we've included the 1ω beam modulation (from detailed patch simulations of the Beamlet system), and have estimated effects from residual 1ω and 2ω light. Beamlet experiments are now being planned to examine the filamentation damage threat to the focussing vessel primary lens, and to address 3ω beam quality and focussability at power levels of interest to NIF.³

Summary:

Detailed simulations of the Beamlet system based on 2 x 2 cm patch models at 1ω and 3ω using Prop92 indicate that the IL product for filamentation damage for crystals with 2-nm or less r.m.s. surface roughness over 10-mm regions should be ~ 36 GW/cm; and for crystals up to 4-nm roughness, ~ 27 GW/cm, based on the nominal 3ω intensity at the exit plane of the crystal array. By "nominal" we refer to the average intensity over any 2 x 2 cm region. Typically 75 % of the total r.m.s. roughness value quoted for the 10-mm aperture occurs over the 120- μ m to 500- μ m scale important for initiating nonlinear filament growth, with PSD shapes typical of current crystal finishes. An estimate for combined illumination with residual 1ω and 2ω light indicates that these thresholds could be reduced by as much as 25% when the 1ω and 2ω filaments or "hot spots" are correlated with the 3ω . This is not such a totally ridiculous assumption, since the more intense 3ω beam will tend to trap the weaker 1ω and 2ω filaments by non-linear self-focussing. Cases were considered with surface roughness up to 8.0-nm r.m.s. In these cases, the threshold is reduced to ~ 20 GW/cm, and could go as low as ~ 16 GW/cm with combined 1ω and 2ω illumination. I'm estimating now that the accuracy of these thresholds for filtered 3ω illumination is about ± 10 %, and is based on the assumption that the filamentation threat is strictly proportional to the IL product. The situation is much more uncertain when we add the residual 1ω and 2ω light.

Additionally, we find that the gap between the doubling and tripling crystals is important. The modulation of the 3ω beam downstream is reduced by 20% with a 10-cm crystal gap, as compared to no gap. The dependence of IL threshold on crystal to lens separation was not studied here; however, the effects are noticeable with the 60-cm gap used on Beamlet. The rise in 3ω peak-to-average modulation at 4 GW/cm² is 1.07 times (1.54 to 1.64) for "good" crystals (2-nm r.m.s.) over this distance, to as much as 1.25 times (1.82 to 2.26) for "rough" crystals (8-nm r.m.s.).

With "rough" crystals, the peak to average modulation at the lens can exceed 3.3 times the nominal intensity at the crystals, and filamentation damage is thus predicted to be observed at ~ 3 cm or less inside the lens.

Table 1 summarizes the basic 1ω and 3ω modulation results for crystals with 4-nm r.m.s. roughness. I list the 1ω average intensity and peak-to-average modulation at the Beamlet crystal location, the cavity B-integral and booster amplifier B-integral values, the 3ω average intensity and modulation at the exit face of the tripling crystal, and at the entrance to the focus lens. Five crystal roughness cases, and one case with no crystal gap were considered at 7-intensity levels, from 0.3 to 6.5 GW/cm² at 1ω . Specific data for each crystal surface case are attached to the figures. The estimated minimum distance to filamentation damage and estimated average and peak IL products are listed for each intensity level. Crystal surface roughness was varied from 2-nm, to 3-nm, 4-nm, 6-nm and up to 8-nm r.m.s (scale factor=4.0). A Prop92 simulation of Beamlet at 1ω was constructed on a 2 x 2 cm grid of 512 x 512 points using Beamlet slab 16 interferometer data⁴ (w 1638e, w1638f, etc.), interferometer data for the spatial filter lenses (BSF38Tc, etc.), Pockel's cell crystal surfaces (3112fra and 3112frc), and 1ω diagnostic beam splitter (BPCDLT38). This data was used to be representative of Beamlet, rather than to model any specific configuration. Some components such as polarizers, cavity mirrors, and Pockel's cell windows are missing in the simulation, and may be available today that were not when I first built the model in 1995. In accord with current full aperture modeling of Beamlet, I scaled all the aberrations up by 1.8 times. Also, so as not to under-estimate the modulation over a 2-cm square patch, I assumed 200- μ R (half-angle) cavity and transport pinholes. The pulse format for these runs was a 700-ps ramped pulse. The seven 100-ps time-slices represent the full range of Beamlet operating intensities (and then some). Fig. 1 shows data plots relevant to the Prop92 run such as the time slice information, the reference (nominal) intensities, the peak intensities, and the peak B-integral values. Fig. 2 shows line-scans along x and y directions through the peak of the 1ω beam at the KDP crystal location. (A 1024 x 1024 point run is shown, which gave near identical results to the 512 x 512 run). We see that the peak-to-ave modulation on the beam increases with nominal intensity level (see Table 1.), and that the "ripple" on the beam appears predominately at a spatial frequency of 5 to 6-mm, which is approximately the laser wavelength divided by the 200- μ R transport pinhole cut-off.

A version of Jerry Auerbach's 4-D crystal conversion code "thg4d01" was used ("convert4d", archived on "Mynx" in /extern/users/henesian/convert4d-src/) that includes diffraction of the fields between crystals, surface aberration scale factors, and other additions to the standard version.⁵ Beamlet's 10.5/9.5-mm type 1/type 2 converter design was assumed. With doubler crystal tuning of 240- μ R (internal) the code predicts conversion efficiencies as high as 88.7% at 3.5 GW/cm² drive intensity, dropping to 83.7% at 6.5 GW/cm². Fig. 3 shows line-scans along x and y through the peak of the 3ω beam at the exit face of the tripling crystal, for the case with 4-nm r.m.s. surface roughness. The high-frequency spatial modulation added by the crystal

surface aberrations and “amplified” by the frequency tripling process, is very apparent. The increase in peak-to-ave modulation is listed in Table 1. The modulation appears to have a higher spatial frequency the along-y direction, the tripler’s ordinary crystal axis, orthogonal to ripples that would arise from interference of waves at angles that effect tripler phase-matching. Fig. 4 shows the 3ω beam at the entrance face of the Beamlet focus lens. The increase in peak-to-ave modulation from propagation over the 60-cm is 8% at low intensity, and up to 22% at high intensity. The spatial-frequency structure of the beam does not appear to change much, except that certain “hot” spots become more pronounced.

For the crystal surfaces, I constructed 2-cm square aberration profiles using Janice Lawson’s code “sim2d.pro”, from 10 x 10 mm interferometer data of a recently diamond-turned 27-cm type II crystal - the same data that we used in the NIF re-optimization design.⁶ The advantage of this approach is that the PSD’s (power spectral densities) of the simulated profiles will be nearly identical to the interferometer data on which they are based, and will be “periodic” over the computational grid. Files 10R2404C1 and 10R2404C3 were used to construct four simulations on a 1024 x 1024 point grid: 10R2404C1_ssm1, 10R2404C1_ssm2, 10R2404C3_ssm1, and 10R2404C3_ssm2. 10R2404C1_ssm1 and 10R2404C3_ssm1 were assigned to the front and back surfaces of the doubler to give a $\sim 30^\circ$ cross-hatched diamond-turning pattern, and 10R2404C1_ssm2 and 10R2404C3_ssm2, rotated by 90° , were used for the tripling crystal. PSD plots of the simulated profile 10R2404C1_ssm1 and interferometer data 10R2404C1 are shown in Fig. 5. The simulations were cut off at 25 ripples/mm, slightly past the Nyquist frequency of the data. Shown in Fig. 6 are PSDs of two 2 x 2-cm simulated profiles for the surface of the Beamlet focus lens, based on interferometer data BFL22R1a for short-scale length, and data file BFL70R1d for the longer-scale aberrations. The aberration profiles were summed together and applied to the beam at the lens entrance face. These files were constructed by R. Sacks and used in recent NIF simulations.⁷

Figures 7 through 12 represent the results of the 3ω filamentation runs. The peak intensity is plotted as a function of distance inside the lens. A data table is attached describing each run. Every 5-mm step in the simulation was subdivided into 10 computational sub-steps to obtain a convergent result. The 1024 x 1024 point crystal files were interpolated by Prop92 down to 512 x 512 points, because of run-time and disk-space limitations on our HP workstations. The resolution was 39.1- μm at a Nyquist angle of 4.49 mrad at 3ω . This gives us 4-sample points across an initially collapsing filament (see below). Notice from the figures that the peak intensity grows with distance up to fairly high intensities (~ 10 -times initial intensity) and then appears to drop or oscillate at a certain distance. Shown in Figs. 13 and 14 for the 4-nm r.m.s. case are Prop92 line-scans through peak intensity at 5-cm into the lens, the minimum distance to collapse at the highest nominal intensity, 5.44 GW/cm², and at 6-

cm into to lens, where we see the appearance of many filaments, at the two highest intensities, 4.73 and 5.44 GW/cm². For Beamlet crystals, with the current surface finish quality, and where we don't expect 3 ω average intensities above 4.0 GW/cm², only very modest intensity growth is observed at 5-cm. Greater than 8-cm of glass is required to have a filamentation damage threat at 4.0 GW/cm², by these calculations.

Close examination of code output at the noted distances shows that the most prominent filament reaches peak intensity, and thereafter, new "hot spots" appear at other locations as the principal one drops in intensity. We think that this is the point at which the principal filament has collapsed in radius below the grid resolution, and thus requires spatial Fourier components outside the allowed numerical K-space, which leads to numerical uncertainty. I've marked the points on the figures at which the intensity falls, and I've conservatively taken these distances to be the minimum distances to collapse, assuming that real filament collapse will happen shortly thereafter. The accuracy of this determination is about ± 5 -mm. We will verify this with higher resolution simulations.

Theory:

Concepts from our current beam filamentation theory can be used to estimate the minimum distance to filament collapse.⁸ We know from BT-ripple growth theory that the angle of highest ripple gain is given by

$$1.) \quad \theta_{opt} = \text{sqrt} (2\gamma I_0 / n_0)$$

where γ is the nonlinear refractive index at frequency ω , which we can label as $\gamma(\omega, \omega)$, n_0 is the linear index, and I_0 is the background or average intensity. We can show that the optimum initial size for beam filaments to grow out of the background irradiance I_0 is

$$2.) \quad d = 1/\kappa_x = \lambda_0 / (n_0 \theta_{opt})$$

where d is the full-width at 1/e diameter of a Gaussian-like spot. The effective area of this spot is $\sim \pi d^2/4$ and will contain ~ 2.7 critical powers P_c for self-focussing, where

$$3.) \quad P_c = \pi (1.22\lambda_0)^2 / (32n_0\gamma).$$

Appreciable nonlinear growth will occur over the range of filament diameters from $d/\sqrt{2}$ to $4d/\sqrt{2}$ at the BT-gain half-power points, containing therefore, 1.35 to 21.6 critical powers per filament. Note that the critical power decreases quadratically with decreasing wavelength, consistent with a linear reduction in filament diameter, which illustrates the increased filamentation damage risk and smaller filament size at 3 ω . In

fused silica the critical power at 3ω is 0.343 MW, and therefore at a nominal intensity I_0 of 4 GW/cm², we could develop a (very large !) filamentation damage track density of $\sim 4000/(2.7*0.343) = 4300$ per cm², in a slab of length greater than $z = (IL)_{th} / I_0$ where $(IL)_{th} \sim 36$ GW/cm.

According to P. L. Sulem, et. al.,⁹ and verified in simulations by J. Trenholme,¹⁰ the initially collapsing filament will reshape itself into a special self-similar beam shape $R(r,z)$ that will then evolve with distance z in the dielectric medium, according to:

$$4.) \quad \psi(r, z) = R(r_0/(z_c - z)^{2/3}) e^{i\phi} / [(z_c - z)^{2/3}]$$

for $z < z_c$, where $\psi(r, z)$ is the electric field envelope, r is the radius, and z_c is the critical distance to collapse given approximately as

$$5.) \quad z_c = 2.3 \lambda_0 / (\pi n_0 \theta_{opt}^2).$$

Considering only the peak on-axis intensity of the collapsing filament, beginning at some reference value I_0 at $z = 0$, we have from Eqn. 4 that,

$$6.) \quad I(z) = I_0 / (1 - z/z_c)^{4/3}.$$

When $I(z)$ exceeds the material breakdown strength (somewhere above 250 GW/cm²), a filamentary damage track will form in the bulk material. As an example, consider a beam with a nominal intensity of 4 GW/cm², so we'll take $I_0 \sim 4$ GW/cm². We calculate a ripple angle of 1.38 mrad and an filament diameter of 171- μ m at the BT-gain peak. Appreciable nonlinear growth will occur over the range of filament sizes from 120- μ m to 500- μ m diameter at the BT-gain half-power points. For reliable simulations we require about 8-sample points across any filament. For the calculations here we have about 4-samples, which only allows partially tracking of the filament collapse. From Eqn. 5 we find that the minimum distance z_c to collapse is ~ 9.1 cm. Inverting Eqn. 6 gives a breakdown distance z_{th} of ~ 8.7 cm at 250 GW/cm², corresponding to an intensity-length product $z_{th} I_0$ of 34.8 GW/cm. The $z_{th} I_0$ product will increase asymptotically to 36.5 GW/cm as I_0 decreases. The surface roughness of crystals, optics, etc. can be factored into these simple estimates, since propagation of the otherwise smooth beam through the "noisy" components will increase our estimate of the intensity I_0 by the modulation ratio, and thus decrease z_{th} .

The equations above are incorporated in our latest release of Prop92, and provide the user an estimate of the damage threat, even when calculations cannot resolve filament collapse. The Prop92 filament damage code attempts to estimate

whether material breakdown could occur at any location prior to the (fictitious) exit surface of each computational slice. This code is based on the self-similarity of the collapsing filament solution, and the idea that Eqns. 5 and 6 can be applied at the (fictitious) entrance surface of every slice, where I_0 is now taken to be the highest intensity or “hot spot” in the field, not just the “nominal” or reference value. Not surprisingly, at the distances indicated in Figures 6 through 12, where the peak intensity first drops or oscillates, Prop92 issued filament damage warnings. In the calculations discussed here, we resolve only the beginnings of filament collapse. But Prop92 warns us that material breakdown will occur within the next 5-mm.

Therefore, I’ve taken the distance where the peak intensity first drops-off to be the approximate length to material breakdown. Multiplying by the nominal 3ω intensity at the tripling crystal exit face, we estimate a threshold for filamentation, based mostly on the data for the last time slice, which has the highest nominal intensity and the shortest distance to collapse. This is probably a pessimistic estimate for the threshold, and assumes (without really good proof) that the threshold depends only on the IL product for specific crystals and geometry. For “good” crystals therefore, we estimate that with a surface roughness of 2-nm r.m.s. or less (which is the current standard), we should be able to stand an IL of ~ 36 GW/cm. This drops to ~ 27 GW/cm with 4-nm r.m.s. crystals, to as low as ~ 20 GW/cm with 8-nm r.m.s. crystals. These conclusions are for single-color illumination, and neglect the nonlinear cross-phase-modulation from the residual 1ω and 2ω light that will also illuminate the lens. We discuss this next.

Estimating Residual Light Effects:

From third-order nonlinear optics theory,¹¹ we can make a “worst” case estimate of this effect. We can derive an expression for the effective nonlinear coefficient $\gamma(3\omega,3\omega)'$ that depends on the usual single-color coefficient $\gamma(3\omega,3\omega)$, the cross-phase-modulation coefficients, $\gamma(3\omega,1\omega)$, and $\gamma(3\omega,2\omega)$, and the ratios η_1 , η_2 and η_3 that describe the “mix” in colors at the Beamlet lens. We take these ratios to be those at the exit face of the tripling crystal, assuming that diffraction from the tripler exit face to the lens input face is a minor effect. For loss less crystals, $\eta_1 + \eta_2 + \eta_3 = 1.0$, by definition, but linear absorption and scatter loss, make this less than one. We also assume that filaments in the the 1ω and 2ω beams are correlated with the same filaments in the 3ω beam. After some basic nonlinear optics derivation we find that

$$7.) \quad \gamma(3\omega,3\omega)' = \gamma(3\omega,3\omega) + 2/3 (\eta_2 / \eta_3) \gamma(3\omega,2\omega) + 2 (\eta_1 / \eta_3) \gamma(3\omega,1\omega)$$

Applying Miller’s dispersion rule¹² (for transparent materials) to the third-order-susceptibilities $\chi(3\omega,3\omega)$, $\chi(3\omega,1\omega)$, and $\chi(1\omega,1\omega)$, we derive that

$$8a.) \quad \chi(3\omega,3\omega) = \Delta_m [(n(3\omega)^2 + 2) / 3]^4 [n(3\omega)^2 - 1]^4$$

$$8b.) \quad \chi(3\omega,1\omega) = \Delta_m [(n(3\omega)^2 + 2) / 3]^2 [n(3\omega)^2 - 1]^2 [(n(1\omega)^2 + 2) / 3]^2 [n(1\omega)^2 - 1]^2$$

$$8c.) \quad \chi(1\omega,1\omega) = \Delta_m [(n(1\omega)^2 + 2) / 3]^4 [n(1\omega)^2 - 1]^4$$

and similarly for $\chi(3\omega,2\omega)$, $\chi(2\omega,2\omega)$, and $\chi(2\omega,1\omega)$, where Δ_m is Miller's coefficient, and the n's are the linear indices of refraction. The nonlinear coefficients $\gamma(3\omega,3\omega)$, $\gamma(3\omega,1\omega)$, and $\gamma(1\omega,1\omega)$ are given in MKSA units by

$$19a.) \quad \gamma(3\omega,3\omega) = 3 \chi(3\omega,3\omega) / [\epsilon_0 c n(3\omega)^2], \text{ and}$$

$$9b.) \quad \gamma(3\omega,1\omega) = 3 \chi(3\omega,1\omega) / [\epsilon_0 c n(3\omega) n(1\omega)]$$

$$9c.) \quad \gamma(1\omega,1\omega) = 3 \chi(1\omega,1\omega) / [\epsilon_0 c n(1\omega)^2]$$

and similarly for the other ter.m.s.. From D. Milam's review article¹³ we'll take the non-linear coefficient at 1ω for fused silica to be $\gamma(1\omega,1\omega) = 2.7 \pm .08 \times 10^{-7} \text{ cm}^2/\text{GW}$.

The best values for the linear indices of fused silica have been compiled by R. English¹⁴ and are $n(1\omega) = 1.449761$, $n(2\omega) = 1.460969$, and $n(3\omega) = 1.476729$. Solving for Miller's delta at 1ω from Eqns. 8c and 9c, and scaling to 2ω and 3ω , we calculate that

$$10a.) \quad \gamma(3\omega,3\omega) = 1.423 \gamma(1\omega,1\omega) = 3.84 \times 10^{-7}$$

$$10b.) \quad \gamma(3\omega,2\omega) = 1.285 \gamma(1\omega,1\omega) = 3.47 \times 10^{-7}$$

$$10c.) \quad \gamma(3\omega,1\omega) = 1.193 \gamma(1\omega,1\omega) = 3.22 \times 10^{-7},$$

For these simulations I've taken $\gamma(3\omega,3\omega) = 3.7 \times 10^{-7} \text{ cm}^2/\text{GW}$ which is the median between the Miller's dispersion estimate above and Milam's recommended value of $3.55 \pm .64 \times 10^{-7} \text{ cm}^2/\text{GW}$. For realistic conversion efficiency conditions, we take η_3 as 0.8, η_1 as 0.1 and η_2 as 0.05, with an assumed 5% total absorption loss. With these numbers we find that

$$11a.) \quad \gamma(3\omega,3\omega)' = \gamma(3\omega,3\omega) [1 + 2/3 (\eta_2 / \eta_3) 1.285/1.423 + 2 (\eta_1 / \eta_3) 1.193/1.423]$$

$$11b.) \quad \gamma(3\omega,3\omega)' = \gamma(3\omega,3\omega) [1 + .0376 + .2096] = 1.25 \gamma(3\omega,3\omega)$$

giving a 25% enhancement in the nonlinear refractive index at 3ω . Under these

conditions, the IL threshold would be reduced to ~22 GW/cm for 4-nm r.m.s. or smoother crystals, and for really “rough” crystals down to ~16 GW/cm.

Conclusions:

Based only on simulations presented here, we can conclude that the Beamlet focusing vessel lens will be safe against filamentation damage at nominal intensities up to 4 GW/cm² (IL threshold ~22 GW/cm) provided that the crystals have surfaces with small-scale roughness less than 4-nm r.m.s. The simulations indicate however, that the threshold for filamentation damage might be lower than expected, as low as ~16 GW/cm with “rough” crystals.

Remaining Issues:

A number of important issues remain to be examined. The effect of distance separating the tripling crystal from the focus lens needs to be explored. We should also consider adjusting the separation between doubling and tripling crystals to lower down-stream intensity modulation. I've assumed that the worst case for surface roughness “build-up” will occur when the diamond turning of the doubler and tripler crystal surfaces are orthogonal. I've also taken the pattern on front and back crystal surfaces to be cross-hatched (by judicious choice of the interferometer files). The various orientation options need to be examined as to their impact on modulation and filamentation threshold. I've also neglected bulk in-homogeneities such as growth sector boundaries prevalent in deuterated KDP crystals. And we've not addressed surface damage issues for longer pulses that are impacted by the diffraction from the KDP surfaces. Calculations should be repeated at higher spatial resolution, ideally on a 1 x 1 cm grid with 1024 x 1024 points. This would quadruple our resolution to 16-sample points per filament, and allow us to observe filament intensities up to about 320 GW/cm², at or above the material breakdown limit, which would give us more confidence in the current predictions. My threshold predictions are purposely pessimistic, since I'm likely under-estimating the distance to filament collapse as a result of spatial resolution limits in these simulations.

The modeling of Dave Milam's recent OSL experiments,¹⁴ by Wade Williams could lead to a higher estimate for the filamentation threshold, as applied to Beamlet of NIF. Wade calculates a peak IL product at threshold of ~68 GW/cm, when scaled by my $\gamma(3\omega,3\omega)$ value, for the case without the obscuring thin-wire in the experimental beam ahead of the fused silica sample. Wade constructed a 1024 x 1024 point model of the 22-mm diameter OSL beam on a 3-cm grid for the simulations. Experimentally, the OSL beam was spatially filtered to separate out the 3ω light and relay-imaged to the fused silica sample to minimize down-stream modulation from the crystals. When peak-to-average modulation, typically 1.5 to 1.8, at the Beamlet focus lens is taken into account, Wade's threshold IL product is reduced to 37 ~ 45 GW/cm for Beamlet. This is on the high-side of the 36 GW/cm value that I estimate for “good” 2-nm r.m.s.

crystals. Increasing the surface roughness to 4-nm r.m.s. and adding residual 1ω and 2ω illumination could reduce this to as low as ~ 22 GW/cm, which would significantly increase the filamentation damage risk to the Beamlet lens.

Acknowledgements:

I thank all the members of the LMO Group for informative discussions on subjects such as optical surface analysis codes, frequency conversion codes, ripple theory, filamentation theory, and NIF patch modeling. Other colleagues from Beamlet, NIF, and LS&T have contributed with valuable discussions on crystal and optical component surfaces, OSL experiments, and Beamlet experiments.

References:

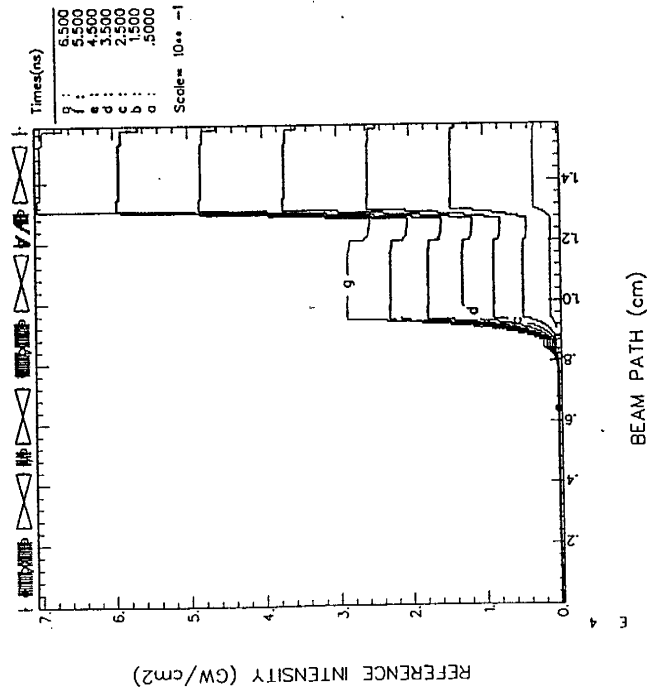
- 1.) R. Montesanti, "Beamlet 37 cm doubler and tripler r.m.s. surface waviness comparisons of one side on each, diamond turned before and after 1995 DTM improvements", compiled April 16, 1996. Data also presented by C. Barker at the Beamlet filamentation group meeting on May 13, 1996.
- 2.) W. Williams, private communications, April 1996.
- 3.) P. J. Wegner, et. al., Beamlet Technology Review presentations, April 24, 1996, to be distributed.
- 4.) C. R. Wolfe, and J. K. Lawson, "Optical component phase maps for laser system modeling and optimization", NIF-LLNL-95-529, L-20495-01, September 27, 1995.
- 5.) J. M. Auerbach, "THG4D01, a New 4D(x,y,z,t) Frequency Conversion Code...", LS&T-LMO95-035, L-20636-01, October 17, 1995.
- 6.) W. Williams, et. al. "The 11-0-7 NIF Laser Design: Description and Background", NIF-LLNL-96-283, L-21804-01, April 10, 1996.
- 7.) R. A. Sacks. et. al. "2D Patch PROP92 Modeling of NIF", NIF-LLNL-96-xxxxxx, L-xxxxx-01, April 12, 1996.
- 8.) J. B. Trenholme, "Overview of Basic Filamentation Concepts", Laser Modeling and Optimization talk, August, 17, 1995, and private communications. See also J. T. Hunt, "A Comparison of Nova and Beamlet's Design Margin Against Beam Filamentation", NIF-LLNL-95-498, L-20374-01, September 18, 1995.
- 9.) P. L. Sulem, C. Sulem, and A. Patera, "Numerical Simulations of Singular Solutions to the Two-Dimensional Cubic Schrodinger Equation", Communications on Pure and Applied Mathematics XXXVII, pp 755-778 (1984), c. 1984 John Wiley & Sons, Inc.

- 10.) J. B. Trenholme, private communications, September-December, 1995.
- 11.) R. W. Hellwarth, "Third-Order Nonlinear Susceptibility of Liquids and Solids", Prog. Quantum Electron. 5, 1 (1977).
- 12.) C. Flytzanis, "Theory of Nonlinear Optical Susceptibilities", Chapter 2 in Quantum Electronics: A Treatise, Vol 1, ed. by H. Rabin and C. L. Tang (1975), Academic Press, specifically see pp. 183-188.
- 13.) D. Milam, "Literature Review - Nonlinear Refractive Index of Silica", LS&T memo, dated December 13, 1995.
- 14.) R. E. English, NIF Optical Design Memo OSE-96-002, March 24, 1996.
- 15.) D. Milam, and W. Sell, "351-nm tracking and induced-image experiments in OSL", CS&T WBS 1.13, LST-BLT96-062/jb, May 18, 1996.

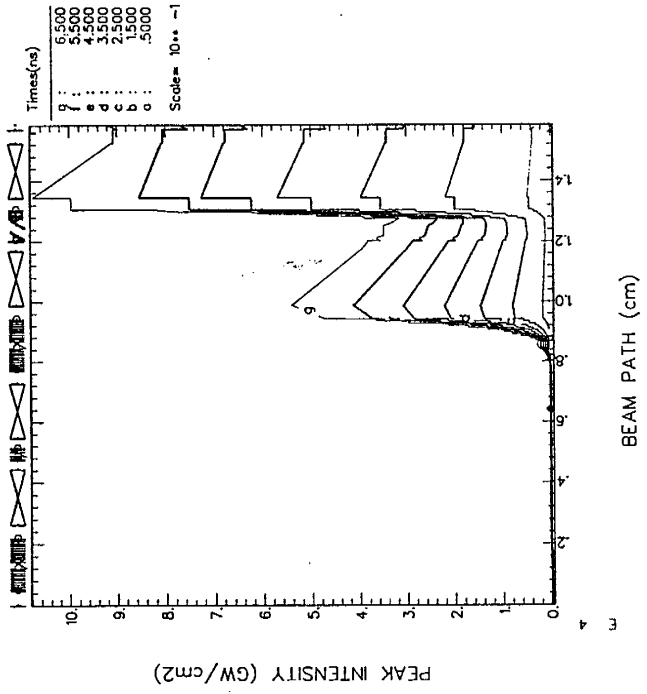
cases:	$\Delta B(\text{cavity})$	$\Delta B(\text{boosters})$	1w Ave. Intens:	1w P/A@kdp	3w Ave. Intens:	3w P/A @kdp	eta=3w/1w
slice 1	0.029	0.087	0.3052	1.0710	0.0416	1.2829	0.136
slice 2	0.132	0.387	1.3520	1.1542	0.8178	1.3407	0.605
slice 3	0.245	0.701	2.4228	1.2563	1.9739	1.4458	0.815
slice 4	0.362	1.025	3.4784	1.3599	3.0856	1.4799	0.887
slice 5	0.496	1.361	4.5165	1.4296	3.9446	1.6241	0.873
slice 6	0.650	1.715	5.5368	1.3959	4.7312	1.7312	0.855
slice 7	0.830	2.092	6.5103	1.4173	5.4491	1.8527	0.837
crystal design: 10.5/9.5-mm KDP/KD*P, 4-nm rms roughness per surface assumed							

Table 1.
1w and 3w modulation results for
crystals with 4-nm rms roughness
surfaces.

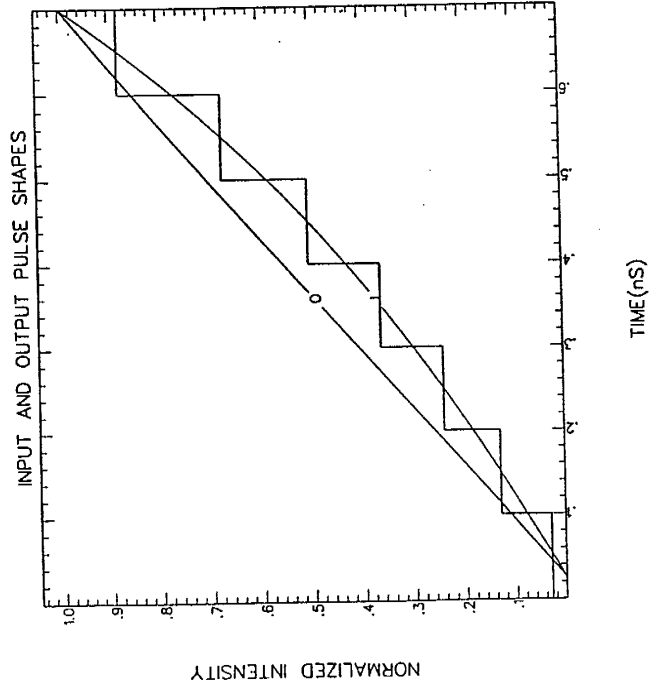
bmlet-patch-ramp-ig: Beamlet,2 x 2-cm Patch



bmlet-patch-ramp-ig: Beamlet,2 x 2-cm Patch



bmlet-patch-ramp-ig: Beamlet,2 x 2-cm Patch



bmlet-patch-ramp-ig: Beamlet,2 x 2-cm Patch

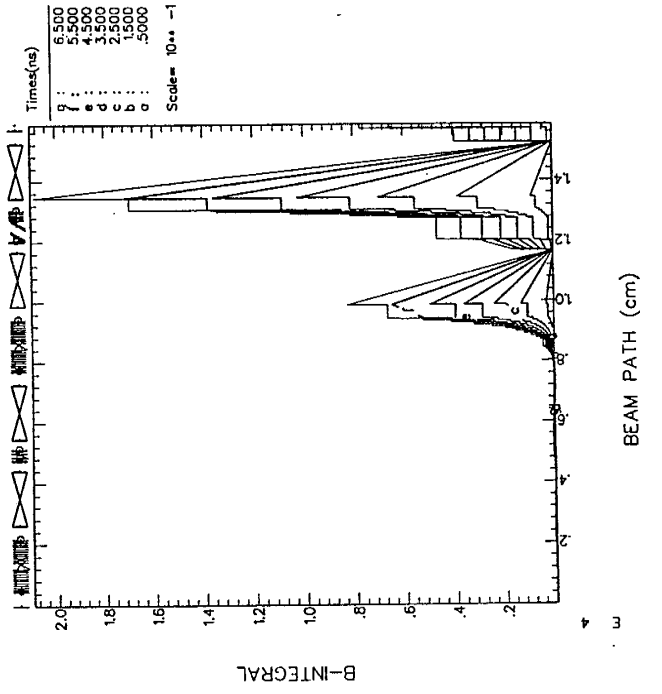
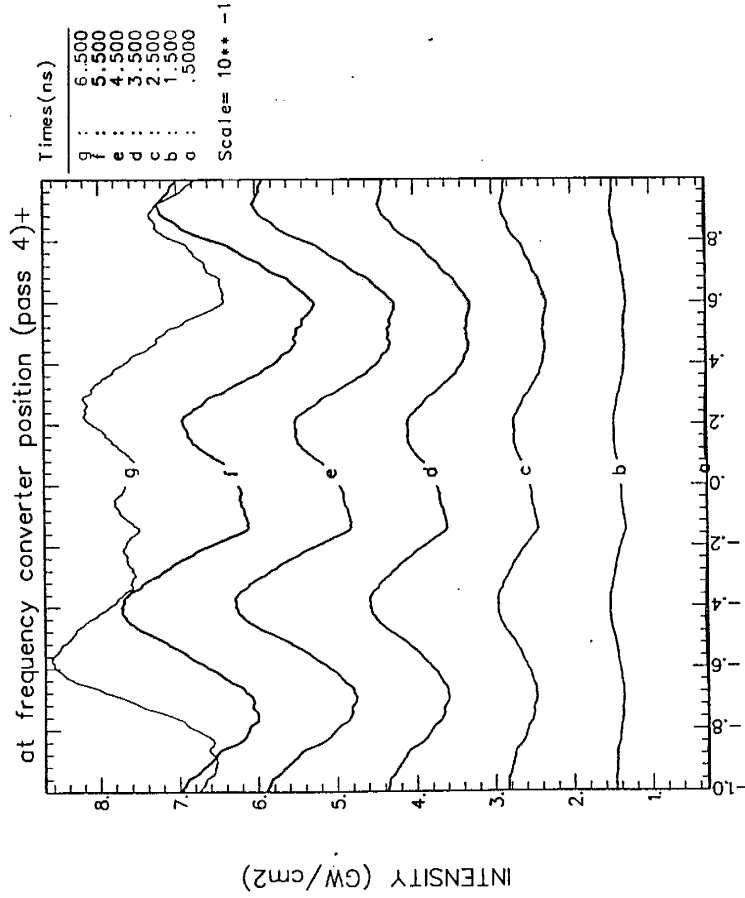


Figure 1.

mlt-patch-ramp-ig: Beamlet,2 x 2-cm Patch

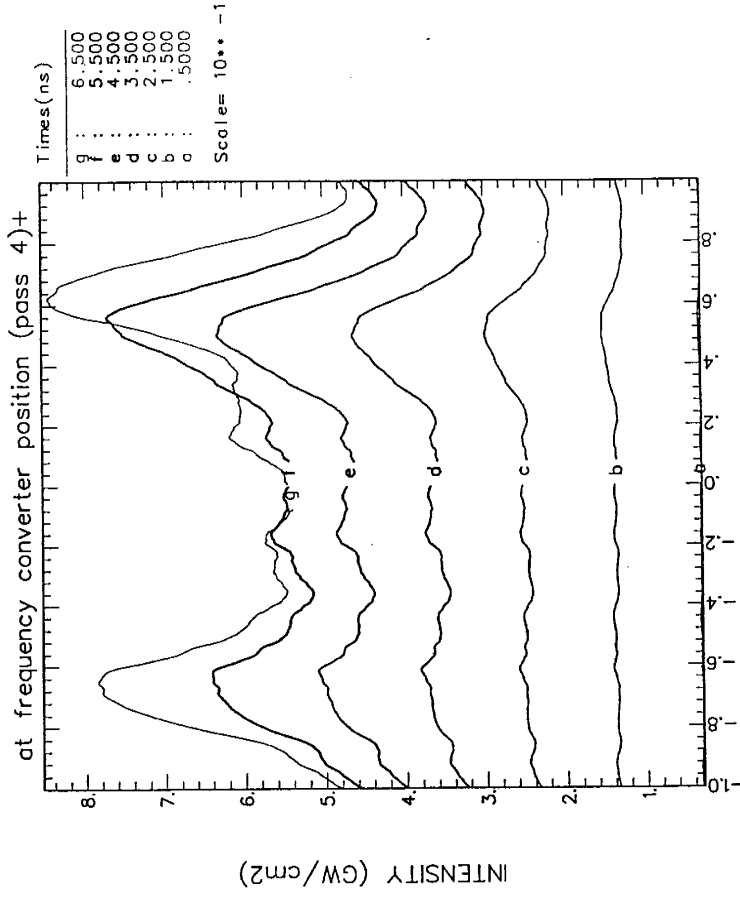


Z COORD = 3947.29 cm
 TOTAL PATH = 15836.0 cm
 MAX B = .772503
 BEAM ENERGY = 9.65010 J
 REF FLUENCE = 2.46633 J/cm²
 REF INT = 6.69429 GW/cm²
 PEAK/REF = 1.40008
 FILL FACTOR = .978308
 LAMBDA = 1.05300 uM

bmlet-patch-ramp-ig.hp146

1024 x 1024 Points, 7 Times
 prop92 Version 2.60b12 16:09:00 23-May-96

ilet-patch-ramp-ig: Beamlet,2 x 2-cm Patch



Z COORD = 3947.29 cm
 TOTAL PATH = 15836.0 cm
 MAX B = .772503
 BEAM ENERGY = 9.65010 J
 REF FLUENCE = 2.46633 J/cm²
 REF INT = 6.69429 GW/cm²
 PEAK/REF = 1.40008
 FILL FACTOR = .978308
 LAMBDA = 1.05300 uM

bmlet-patch-ramp-ig.hp147

1024 x 1024 Points, 7 Times
 prop92 Version 2.60b12 16:09:00 23-May-96

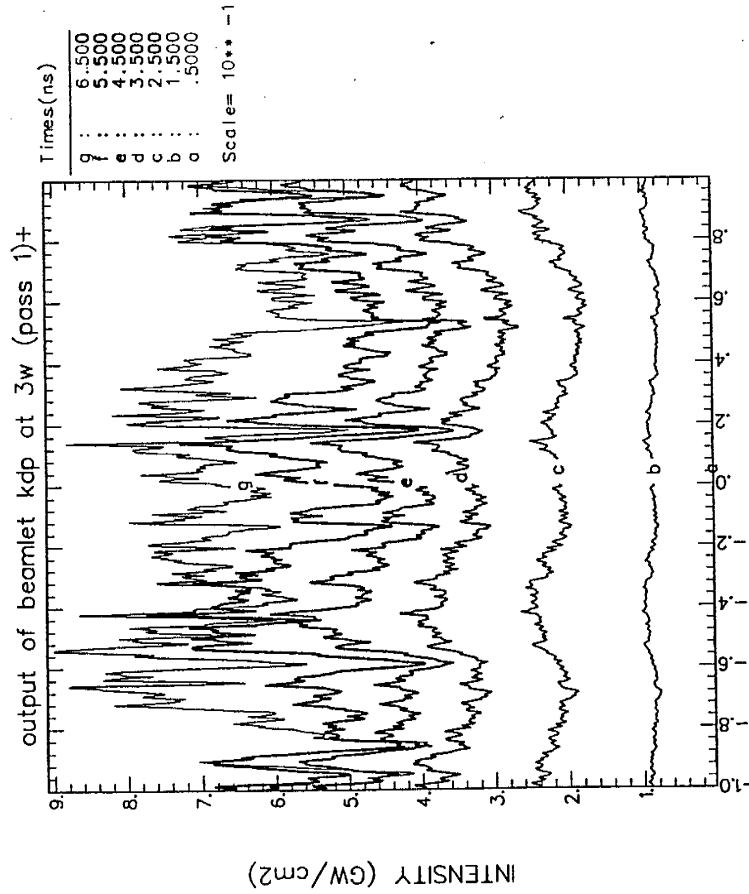
CUT AT X = -.420

Y (cm)

X (cm)

Figure 2.

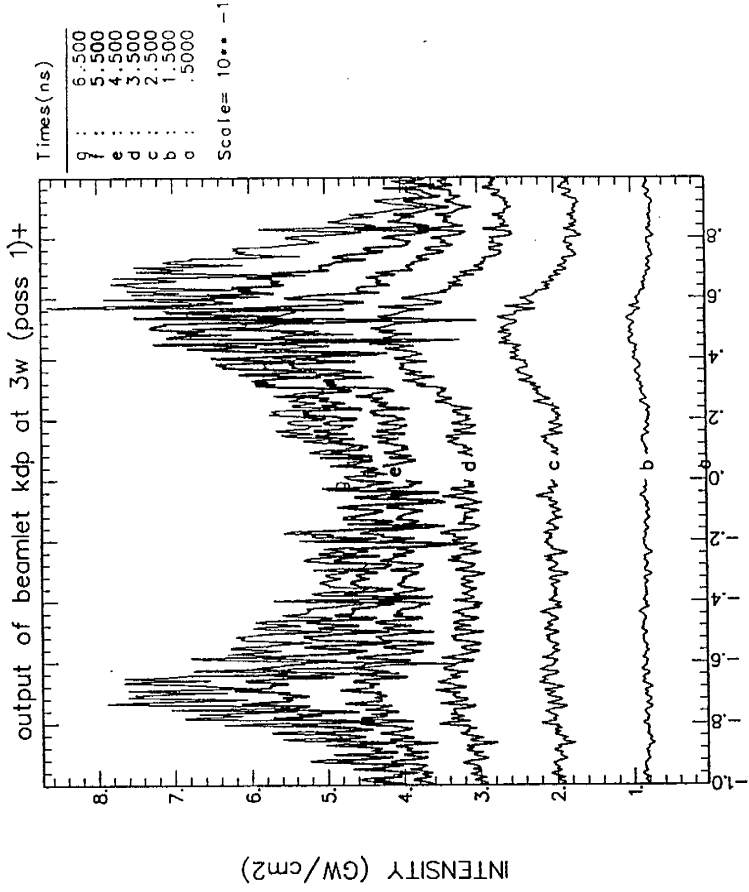
blt-patch-gap-f12B: Beamlet Patch Model,10-cm crystal gap,2.0-X scale



Z COORD = .000000 cm
 TOTAL PATH = .000000 cm
 MAX B = .000000
 BEAM ENERGY = 8.01750 J
 REF FLUENCE = 1.94320 J/cm 2
 REF INT = 5.13048 GW/cm 2
 PEAK/REF = 1.96829
 FILL FACTOR = 1.03149
 LAMBDA = .351000 uM

blt-patch-gap-f12B.hp002 512 x 512 Points, 7 Times
 prop92 Version 2.60b12 20:25:19 23-May-96

blt-patch-gap-f12B: Beamlet Patch Model,10-cm crystal gap,2.0-X scale

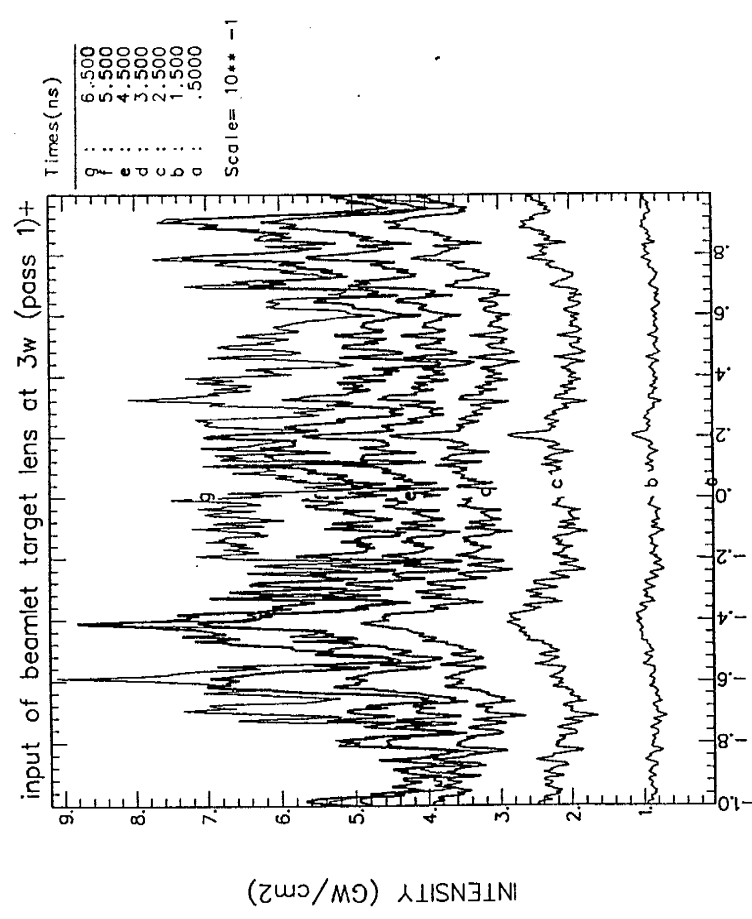


Z COORD = .000000 cm
 TOTAL PATH = .000000 cm
 MAX B = .000000
 BEAM ENERGY = 8.01750 J
 REF FLUENCE = 1.94320 J/cm 2
 REF INT = 5.13048 GW/cm 2
 PEAK/REF = 1.96829
 FILL FACTOR = 1.03149
 LAMBDA = .351000 uM

blt-patch-gap-f12B.hp003 512 x 512 Points, 7 Times
 prop92 Version 2.60b12 20:25:19 23-May-96

Figure 3.

mlet-patch-gap-fl2B: Beamlet Patch Model,10-cm crystal gap,2.0-X scale



X (cm)

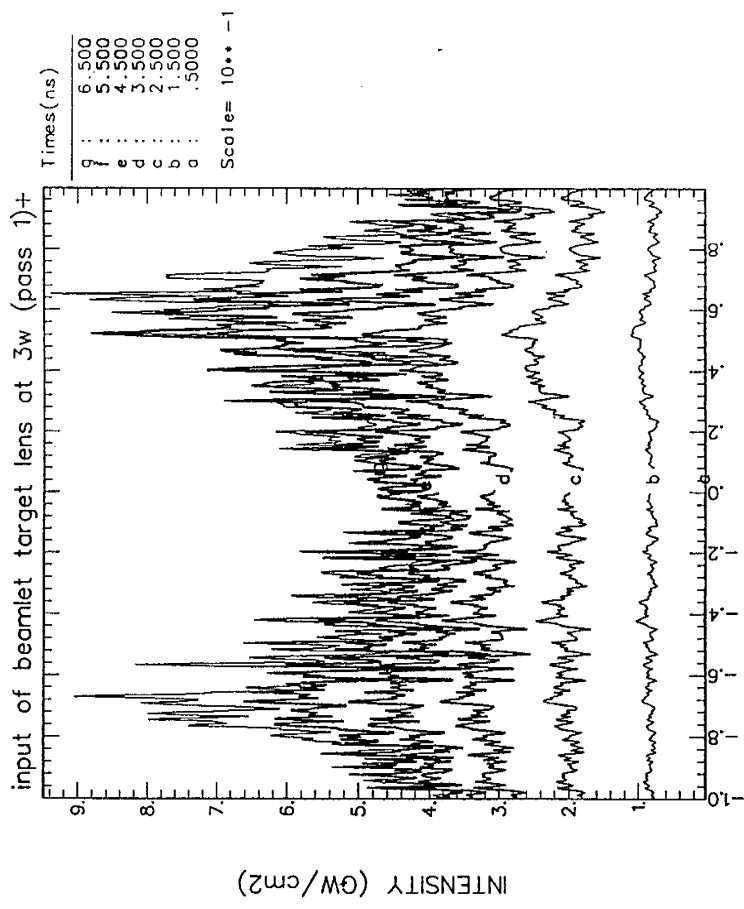
Z COORD = 60.0000 cm
 TOTAL PATH = 60.0000 cm
 MAX B = .000000
 BEAM ENERGY = 8.01746 J
 REF FLUENCE = 1.94320 J/cm 2
 REF INT = 5.13048 GW/cm 2
 PEAK/REF = 2.33783
 FILL FACTOR = 1.03149
 LAMBDA = .351000 uM

CUT AT Y = .523

512 x 512 Points, 7 Times
 prop92 Version 2.60b12 20:25:19 23-May-96

bmlet-patch-gap-fl2B.hp004

mlet-patch-gap-fl2B: Beamlet Patch Model,10-cm crystal gap,2.0-X scale



Y (cm)

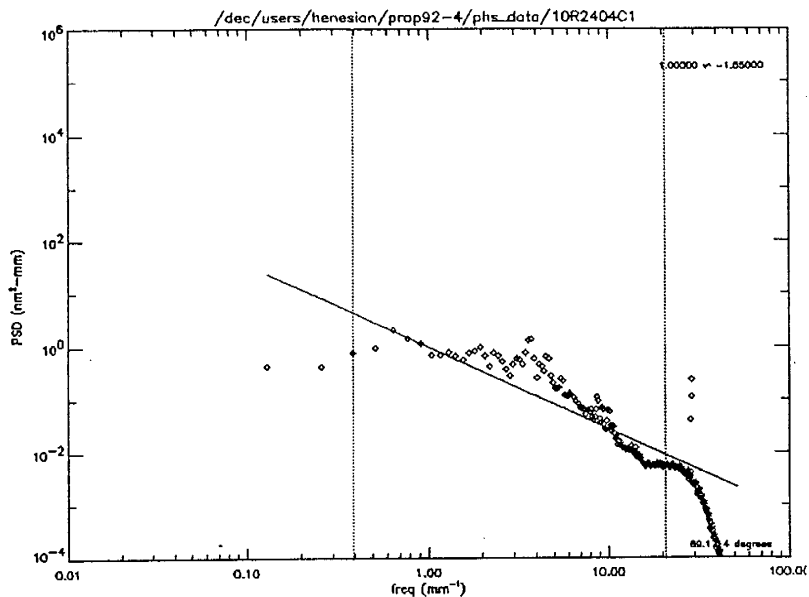
Z COORD = 60.0000 cm
 TOTAL PATH = 60.0000 cm
 MAX B = .000000
 BEAM ENERGY = 8.01746 J
 REF FLUENCE = 1.94320 J/cm 2
 REF INT = 5.13048 GW/cm 2
 PEAK/REF = 2.33783
 FILL FACTOR = 1.03149
 LAMBDA = .351000 uM

CUT AT X = -.410

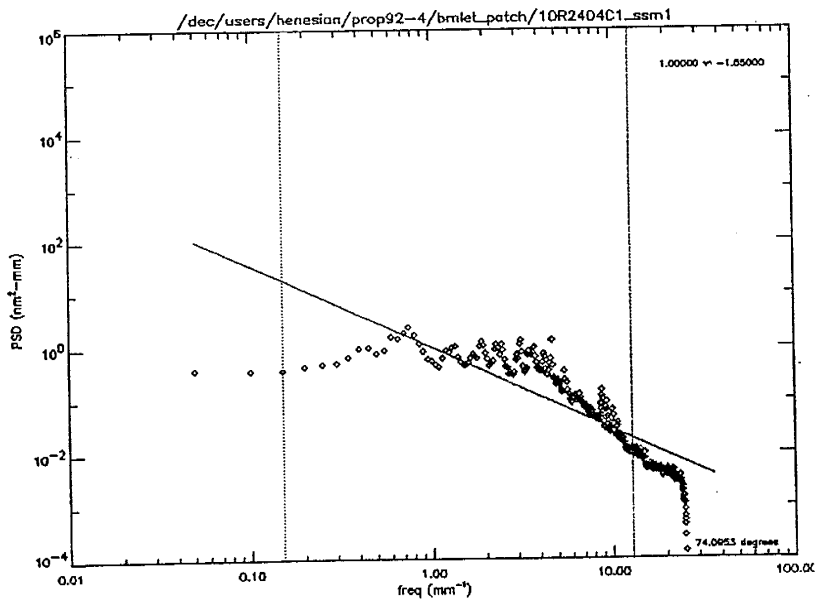
512 x 512 Points, 7 Times
 prop92 Version 2.60b12 20:25:19 23-May-96

bmlet-patch-gap-fl2B.hp005

Figure 4.

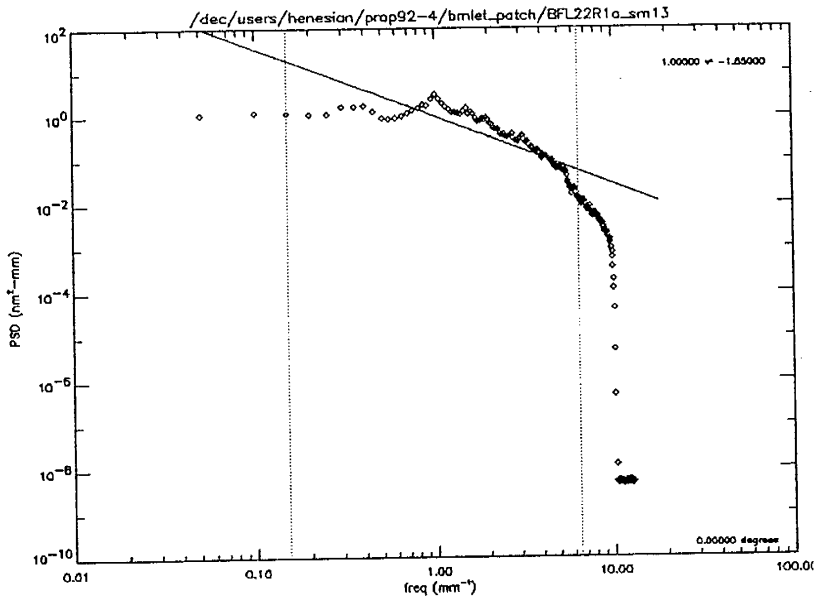


File - /dec/users/henesian/prop92-4/phs_data/10R2404C1
 PV = 29.1411 nm 640,480 pts starting at x,y (mm) -4.99970,-3.74977
 RMS INFORMATION
 total rms (in nm) = 2.01791(z) vs 2.01743(PSD)
 Data valid range (in mm⁻¹) - x,y : 0.300487 - 15.9759 0.400859 - 15.9676
 *1.95303 nm rms in data valid range *
 L<.12 mm .5<L<.12mm 6<L<0.5mm 33<L<6mm 33mm<L
 rms(nm) 0.681541 1.51539 1.14242 0.0840164 4.29808e-07

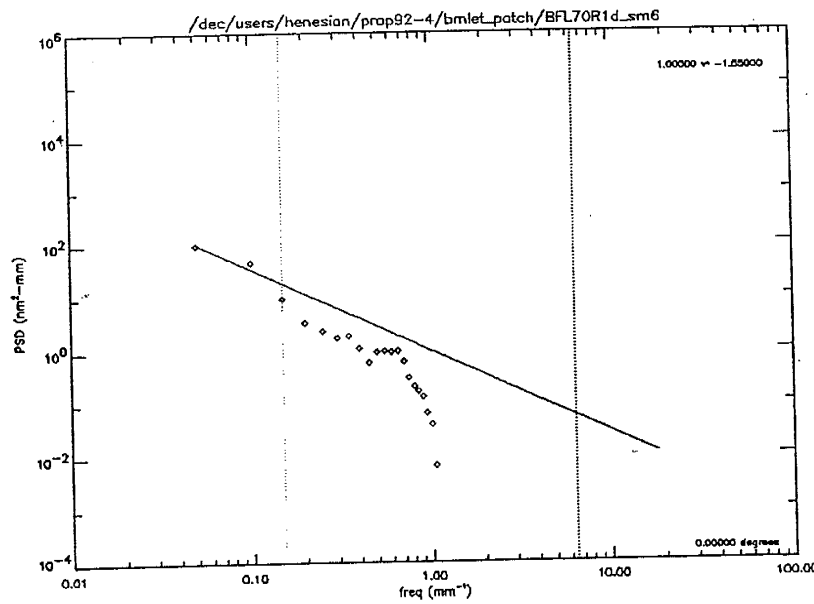


File - /dec/users/henesian/prop92-4/bmlet_patch/10R2404C1_ssm1
 PV = 17.6788 nm 1024,1024 pts starting at x,y (mm) -9.98397,-9.97846
 RMS INFORMATION
 total rms (in nm) = 1.98830(z) vs 1.98770(PSD)
 Data valid range (in mm⁻¹) - x,y : 0.150388 - 12.8080 0.150471 - 12.8151
 *1.96396 nm rms in data valid range *
 L<.12 mm .5<L<.12mm 6<L<0.5mm 33<L<6mm 33mm<L
 rms(nm) 0.566256 1.53098 1.13594 0.0560024 7.27201e-08

Figure 5.

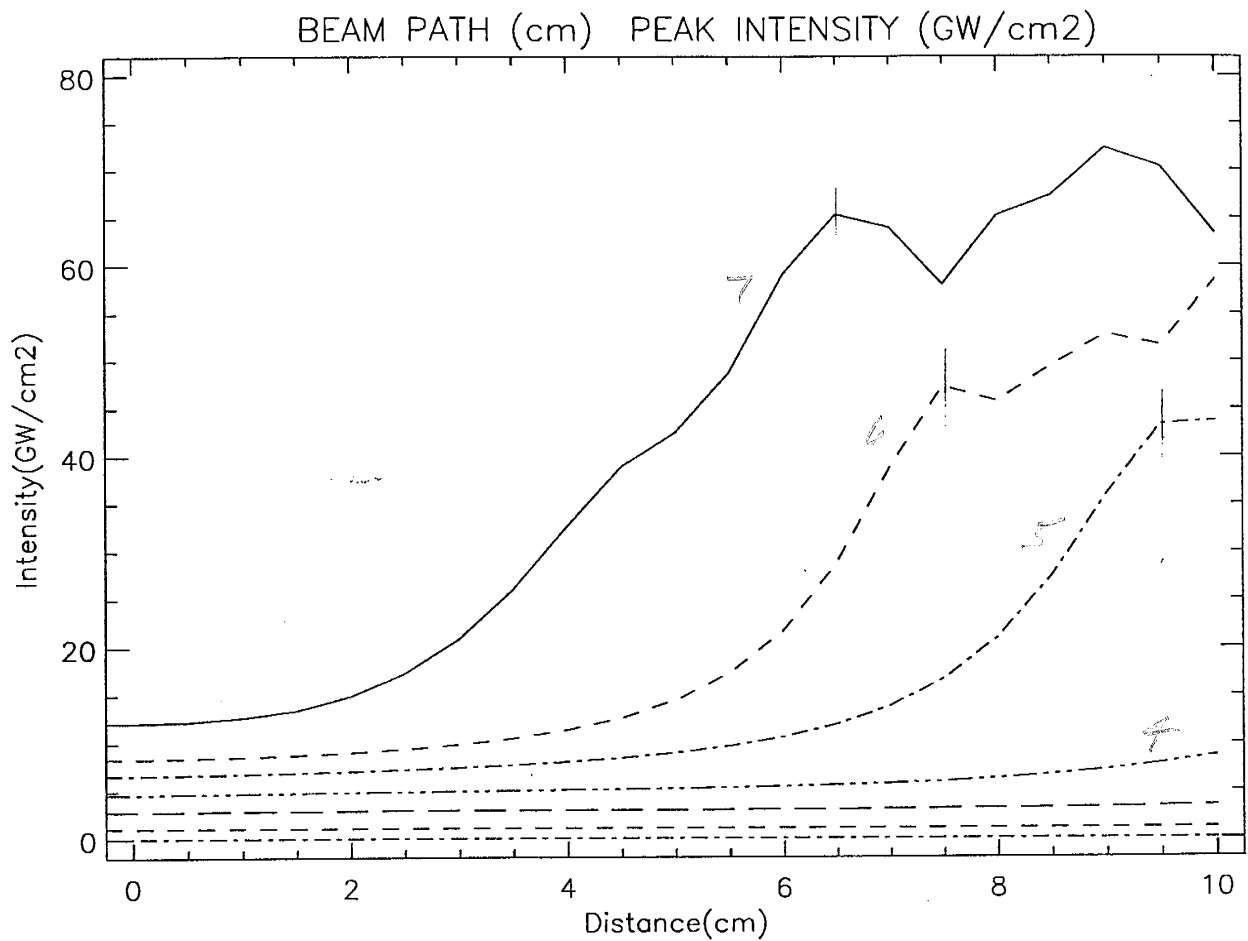


File - /dec/users/henesian/prop92-4/bmlet_patch/BFL22R1a_sm13
 P/V = 16.7024 nm 512,512 pts starting at x,y (mm) -9.97953,-9.96560
 RMS INFORMATION
 total rms (in nm) = 1.86348(z) vs 1.86365(PSD)
 Data valid range (in mm⁻¹) - x,y : 0.150602 - 6.40058 0.150812 - 6.40952
 *1.83816 nm rms in data valid range *
 L<.12 mm .5<L<.12mm 6<L<0.5mm 33<L<6mm 33mm<L
 rms(nm) 0.207366 1.24204 1.37396 4.92847e-06 8.93982e-09



File - /dec/users/henesian/prop92-4/bmlet_patch/BFL70R1d_sm6
 P/V = 23.0891 nm 512,512 pts starting at x,y (mm) -10.0000,-10.0000
 RMS INFORMATION
 total rms (in nm) = 3.57469(z) vs 3.57584(PSD)
 Data valid range (in mm⁻¹) - x,y : 0.150294 - 6.38749 0.150294 - 6.38749
 *2.98072 nm rms in data valid range *
 L<.12 mm .5<L<.12mm 6<L<0.5mm 33<L<6mm 33mm<L
 rms(nm) 2.52055e-05 3.21153e-05 2.29781 2.73983 1.51106e-06

Figure 6.



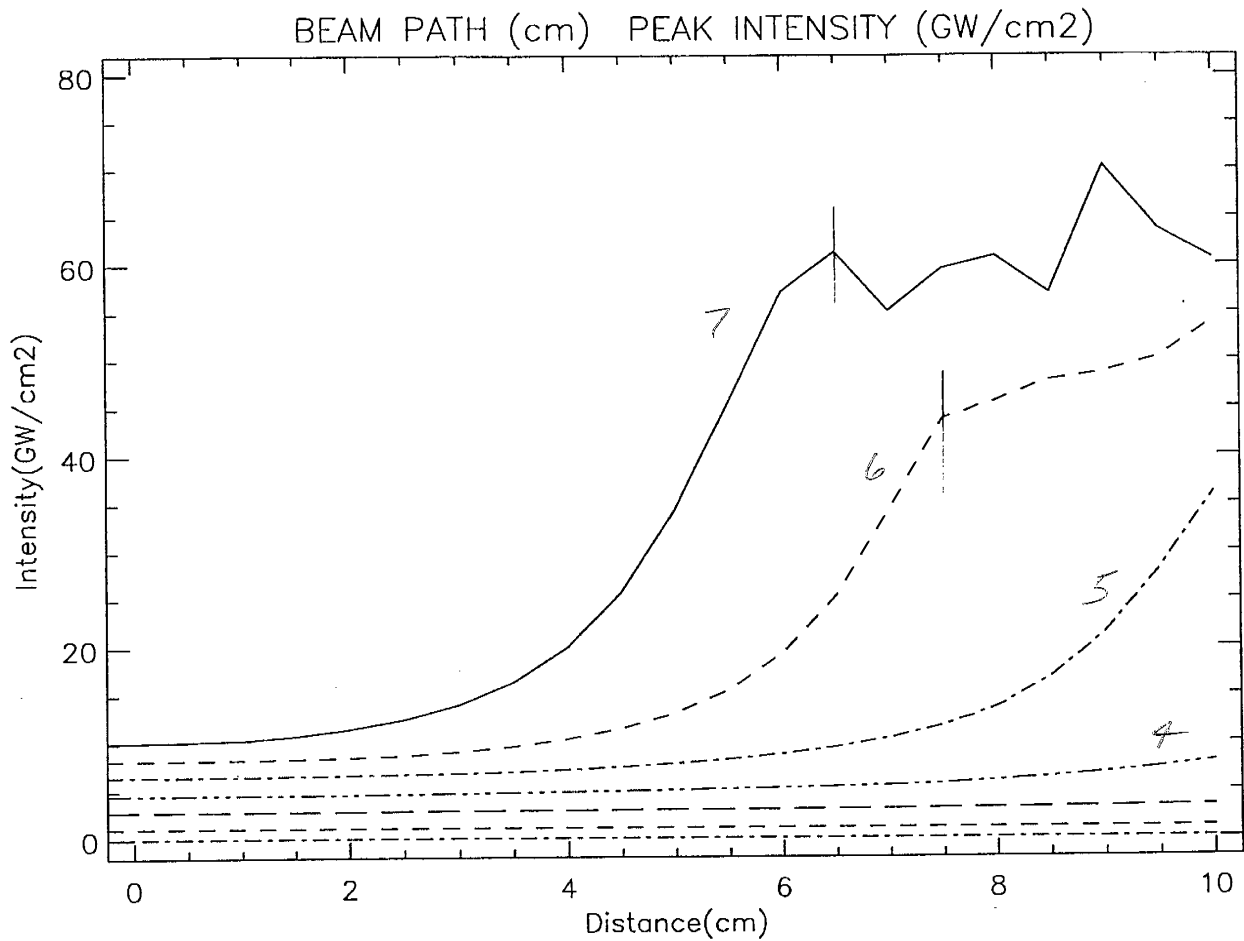
bmlet-patch-ngap-fl2: Beamlet Patch Model, no crystal gap

Case 1.

no crystal gap
 2.0-nm rms roughness per KDP surface
 $\gamma = 3.7 \times 10^{-7} \text{ cm}^2/\text{GW}$

	no crystal gap, 2-nm rms					
	3w Ave. Intens.	P/A @kdp	P/A @60-cm	Min. Dist. (cm)	Peak IL	Ave. IL
slice 1	0.0416	1.1916	1.2586	---		
slice 2	0.8188	1.2761	1.3331	---		
slice 3	1.9782	1.4013	1.4589	---		
slice 4	3.0964	1.4445	1.5252	---		
slice 5	3.9653	1.5831	1.6961	9.5	63.9	37.7
slice 6	4.7749	1.6343	1.7666	7.5	63.3	35.8
slice 7	5.5467	1.6128	2.2145	6.5	79.8	36.1

Figure 7.



bmlet-patch-gap-fl2: Beamlet Patch Model, 10-cm crystal gap

Case 2.

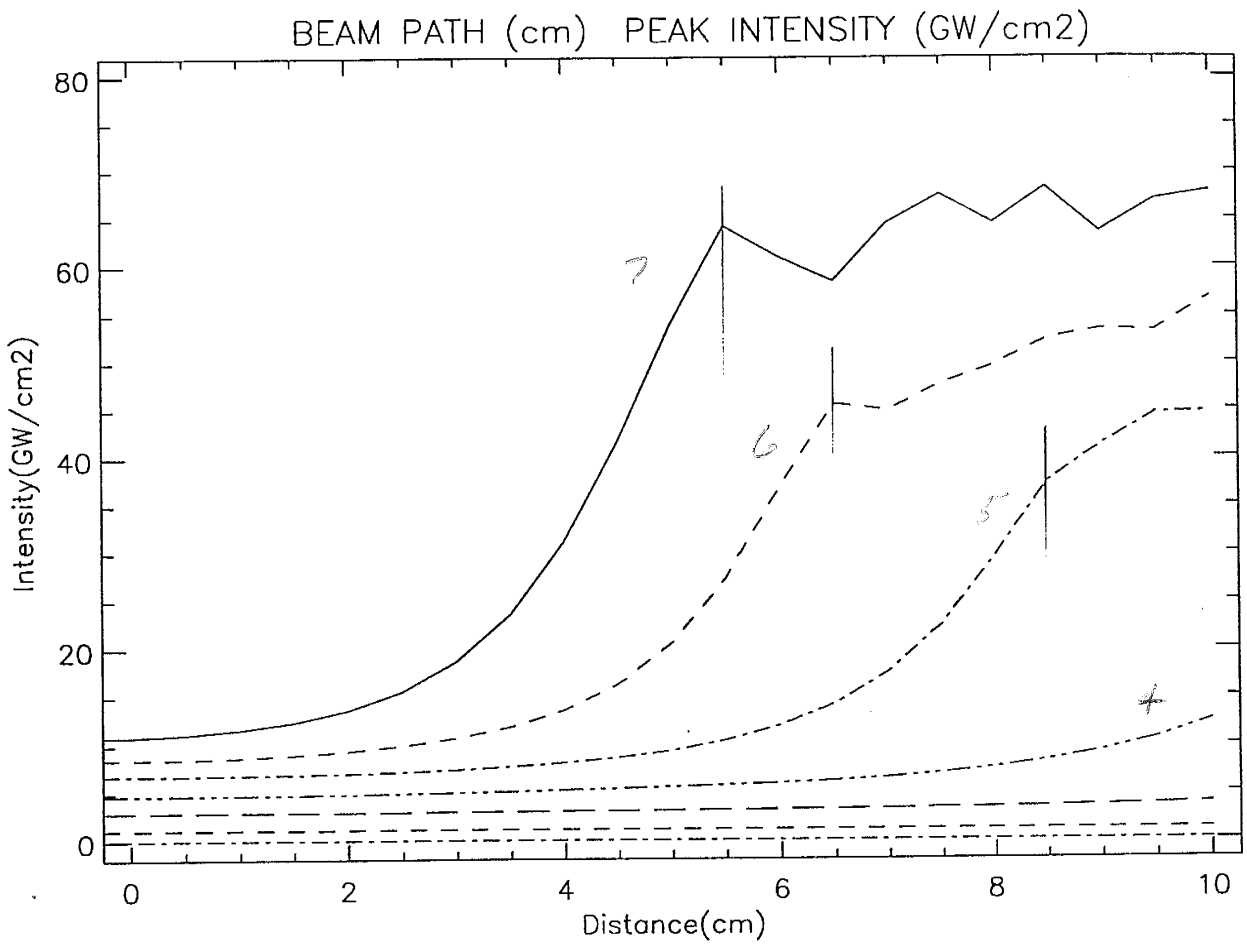
10-cm crystal gap

2.0-nm rms roughness per KDP surface

$\gamma = 3.7 \times 10^{-7} \text{ cm}^2/\text{GW}$

	10-cm crystal gap, 2-nm rms					
	3w Ave. Intens.	P/A @kdp	P/A@60-cm	Min. Dist. (cm)	Peak IL	Ave. IL
slice 1	0.0416	1.2210	1.2648	---		
slice 2	0.8187	1.2862	1.3434	---		
slice 3	1.9779	1.3883	1.4546	---		
slice 4	3.0965	1.4018	1.4824	---		
slice 5	3.9670	1.5403	1.6434	---		
slice 6	4.7805	1.6258	1.7249	7.5	61.8	35.9
slice 7	5.5585	1.6430	1.8344	6.5	66.3	36.1

Figure 8.



bmlet-patch-gap-fl2A: Beamlet Patch Model, 10-cm crystal gap, 1.5X scale

Case 3.

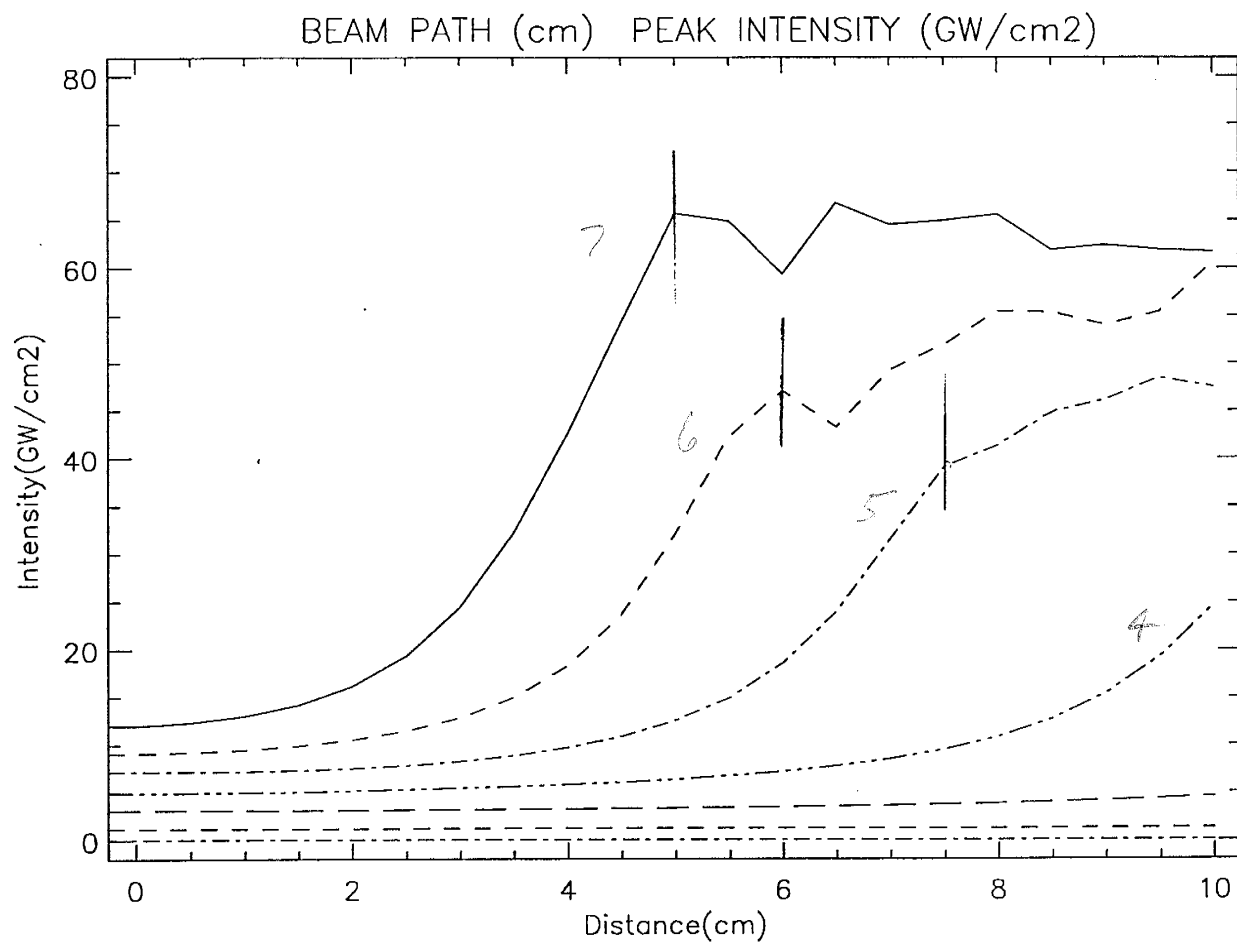
10-cm crystal gap

3.0-nm rms roughness per KDP surface

$\gamma = 3.7 \times 10^{-7} \text{ cm}^2/\text{GW}$

	10-cm crystal gap, 3-nm rms					
	3w Ave. Intens:	P/A @kdp	P/A@60-cm	Min. Dist. (cm)	Peak IL	Ave. IL
slice 1	0.0416	1.2504	1.3225	---		
slice 2	0.8183	1.3129	1.4005	---		
slice 3	1.9763	1.4175	1.5145	---		
slice 4	3.0920	1.4418	1.5436	---		
slice 5	3.9577	1.5847	1.7282	8.5	58.1	33.6
slice 6	4.7598	1.6715	1.7992	6.5	55.7	30.9
slice 7	5.5120	1.7572	2.0264	5.5	61.4	30.3

Figure 9.



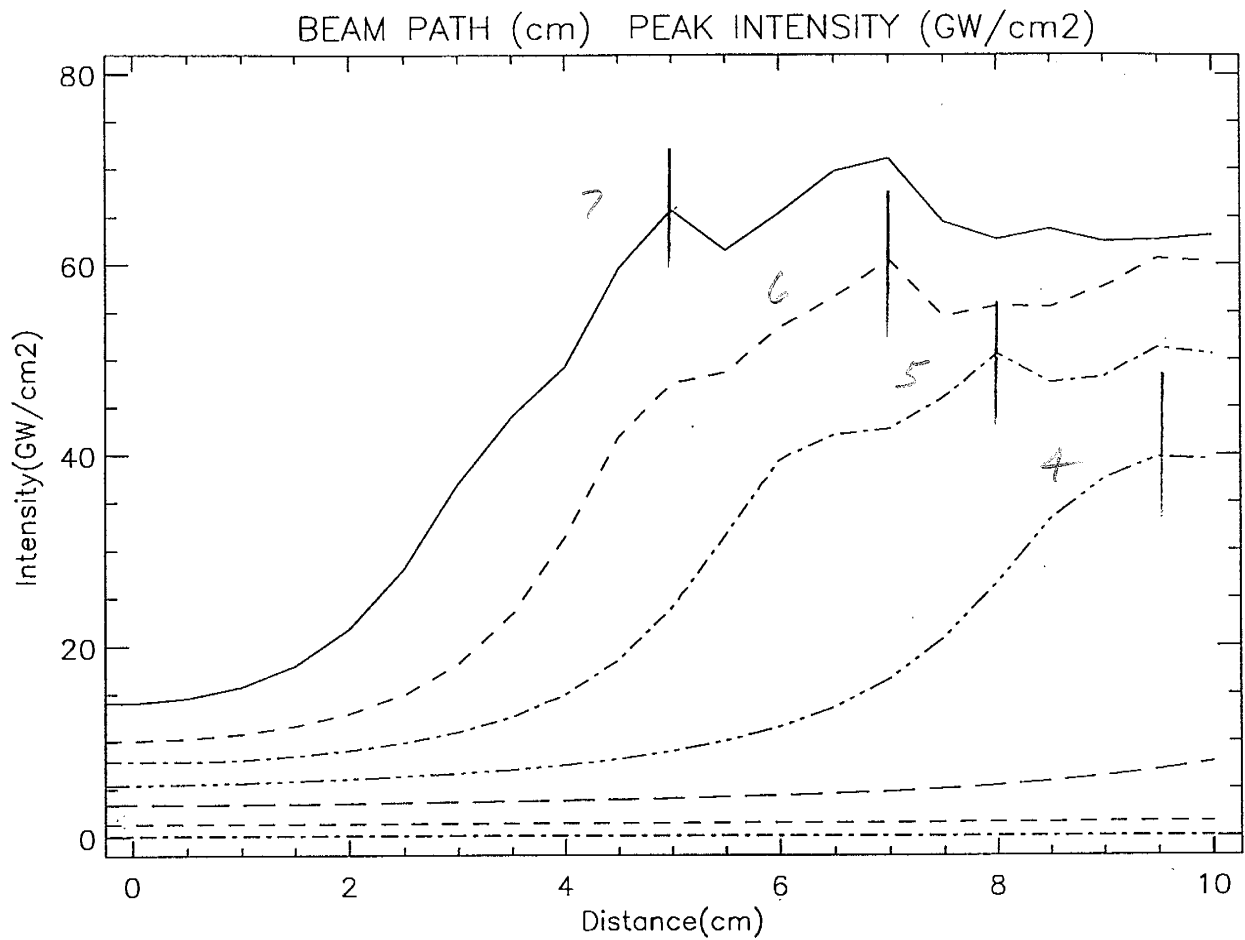
bmlet-patch-gap-fl2B: Beamlet Patch Model, 10-cm crystal gap, 2.0-X scale

Case 4.

10-cm crystal gap
 4.0-nm rms roughness per KDP surface
 $\gamma = 3.7 \times 10^{-7} \text{ cm}^2/\text{GW}$

	10-cm crystal gap, 4-nm rms					
	3w Ave. Intens.	P/A @kdp	P/A @60-cm	Min. Dist. (cm)	Peak IL	Ave. IL
slice 1	0.0416	1.2829	1.3975	---		
slice 2	0.8178	1.3407	1.4589	---		
slice 3	1.9739	1.4458	1.5748	---		
slice 4	3.0856	1.4799	1.6072	---		
slice 5	3.9446	1.6241	1.8083	7.5	53.5	29.6
slice 6	4.7312	1.7312	1.9394	6	55.1	28.4
slice 7	5.4491	1.8527	2.2632	5	61.7	27.2

Figure 10.



bmlet-patch-gap-fl2C: Beamlet Patch Model, 10-cm crystal gap, 3.0-X scale

Case 5.

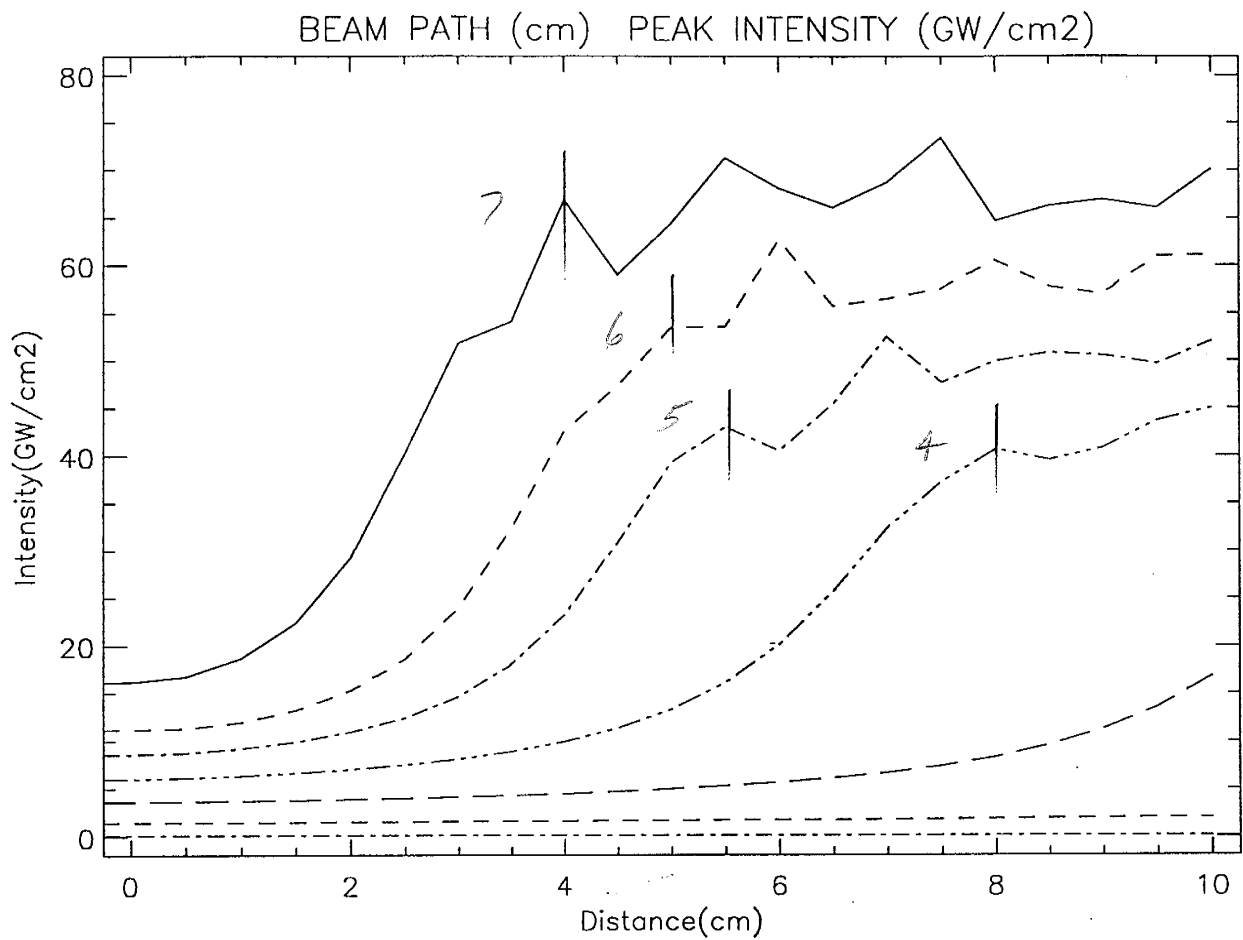
10-cm crystal gap

6.0-nm rms roughness per KDP surface

$\gamma = 3.7 \times 10^{-7} \text{ cm}^2/\text{GW}$

	10-cm crystal gap, 6-nm rms					
	3w Ave. Intens.	P/A @kdp	P/A@60-cm	Min. Dist. (cm)	Peak IL	Ave. IL
slice 1	0.0415	1.3475	1.5517	---		
slice 2	0.8163	1.4059	1.5899	---		
slice 3	1.9672	1.5260	1.6991	---		
slice 4	3.0675	1.5577	1.7915	9.5	52.2	29.1
slice 5	3.9075	1.7115	2.0137	8	62.9	31.3
slice 6	4.6509	1.8569	2.2147	7	72.1	32.6
slice 7	5.2812	1.9662	2.7567	5	72.8	26.4

Figure 11.



bmlet-patch-gap-fl2D: Beamlet Patch Model, 10-cm crystal gap, 4.0-X scale

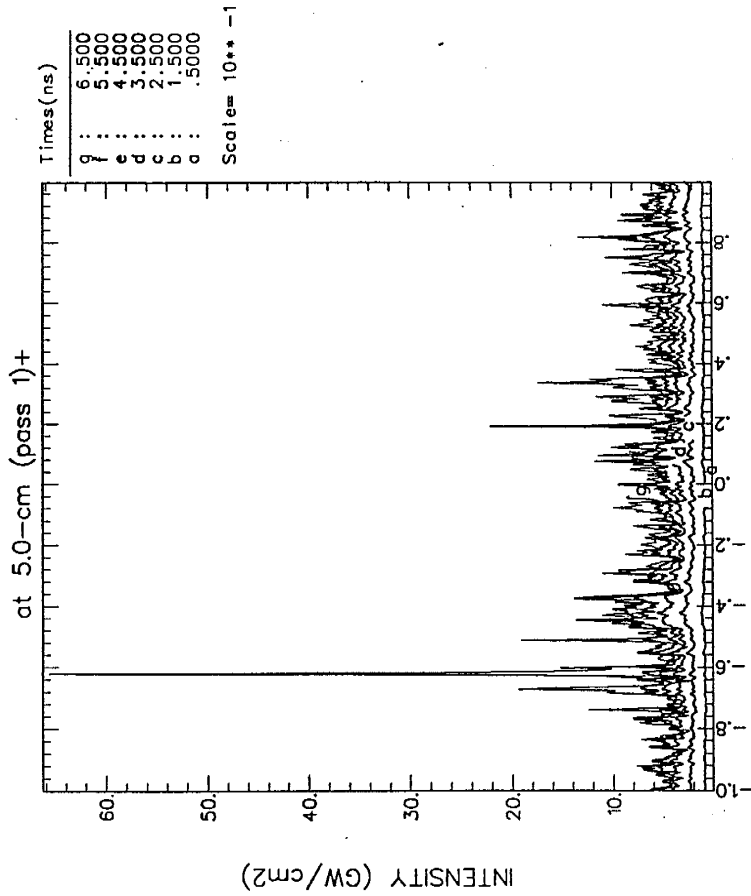
Case 6.

10-cm crystal gap
 8.0-nm rms roughness per KDP surface
 $\gamma = 3.7 \times 10^{-7} \text{ cm}^2/\text{GW}$

	10-cm crystal gap, 8-nm rms					
	3w Ave. Intens.	P/A @kdp	P/A@60-cm	Min. Dist. (cm)	Peak IL	Ave. IL
slice 1	0.0415	1.4147	1.7160	---		
slice 2	0.8142	1.4739	1.7673	---		
slice 3	1.9579	1.6124	1.8746	---		
slice 4	3.0426	1.6444	2.0174		8	49.1
slice 5	3.8565	1.8178	2.2628	5.5	48	21.2
slice 6	4.5431	1.9917	2.4850	5	56.4	22.7
slice 7	5.0705	2.2083	3.3016	4	67	20.3

Figure 12.

ilnet-patch-gap-f12B: Beamlet Patch Model,10-cm crystal gap,2.0-X scale

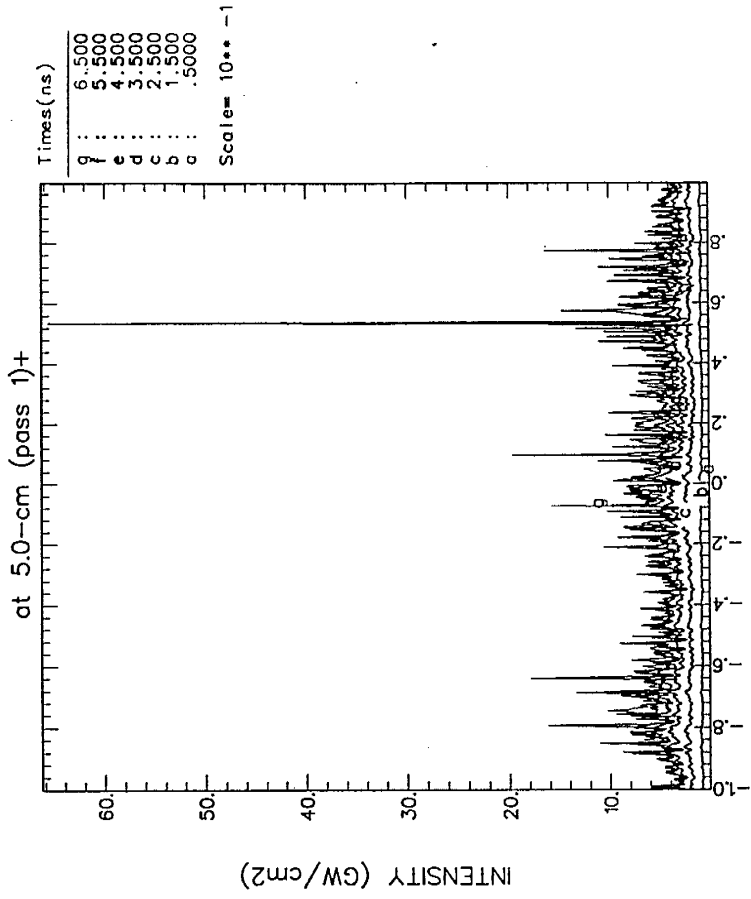


Z COORD = 65.0000 cm
 TOTAL PATH = 65.0000 cm
 MAX B = 1.69903
 BEAM ENERGY = 8.01744 J
 REF FLUENCE = 1.94320 J/cm 2
 REF INT = 5.13048 GW/cm 2
 PEAK/REF = 12.8008
 FILL FACTOR = 1.03148
 LAMBDA = .351000 uM

bmlet-patch-gap-f12B.hp024

512 x 512 Points, 7 Times
 prop92 Version 2.60b12 20:25:19 23-May-96

nllet-patch-gap-f12B: Beamlet Patch Model,10-cm crystal gap,2.0-X scale



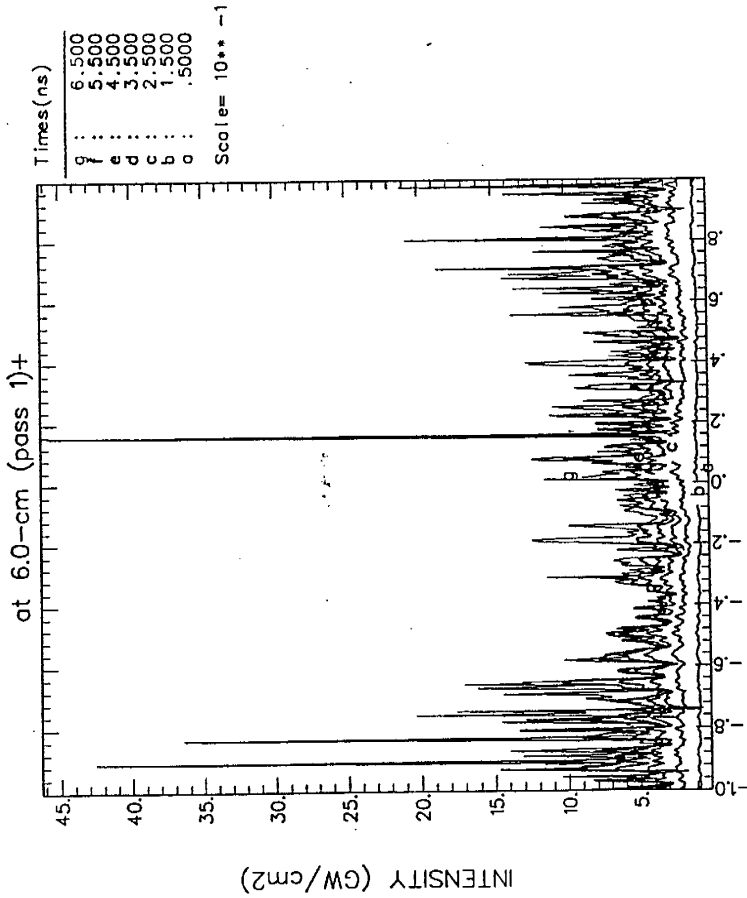
Z COORD = 65.0000 cm
 TOTAL PATH = 65.0000 cm
 MAX B = 1.69903
 BEAM ENERGY = 8.01744 J
 REF FLUENCE = 1.94320 J/cm 2
 REF INT = 5.13048 GW/cm 2
 PEAK/REF = 12.8008
 FILL FACTOR = 1.03148
 LAMBDA = .351000 uM

bmlet-patch-gap-f12B.hp025

512 x 512 Points, 7 Times
 prop92 Version 2.60b12 20:25:19 23-May-96

Figure 13.

nlet-patch-gap-f12B: Beamlet Patch Model,10-cm crystal gap,2.0-X scale



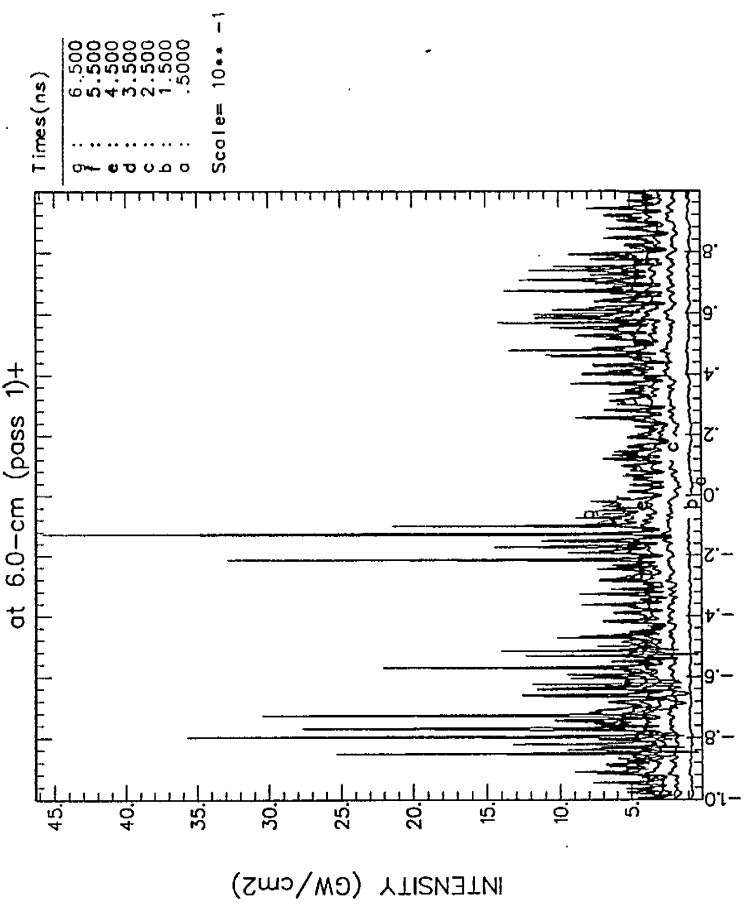
X (cm)

Z COORD = 66.0001 cm
 TOTAL PATH = 66.0000 cm
 MAX B = 2.03884
 BEAM ENERGY = 8.01748 J
 REF FLUENCE = 1.94320 J/cm 2
 REF INT = 5.13048 GW/cm 2
 PEAK/REF = 11.5700
 FILL FACTOR = 1.03147
 LAMBDA = .351000 uM

bmlet-patch-gap-f12B.hp028

512 x 512 Points, 7 Times
 prop92 Version 2.60b12 20:25:19 23-May-96

nlet-patch-gap-f12B: Beamlet Patch Model,10-cm crystal gap,2.0-X scale



Y (cm)

Z COORD = 66.0001 cm
 TOTAL PATH = 66.0000 cm
 MAX B = 2.03884
 BEAM ENERGY = 8.01748 J
 REF FLUENCE = 1.94320 J/cm 2
 REF INT = 5.13048 GW/cm 2
 PEAK/REF = 11.5700
 FILL FACTOR = 1.03147
 LAMBDA = .351000 uM

bmlet-patch-gap-f12B.hp029

512 x 512 Points, 7 Times
 prop92 Version 2.60b12 20:25:19 23-May-96

Figure 14.

Distribution:

G. Albrecht	L-590
J. Auerbach	L-490
S. Burkhart	L-490
E. M. Campbell	L-466
J. Caird	L-495
J. Davin	L-490
G. Deis	L-465
S. Dixit	L-439
D. Eimerl	L-466
E. English	L-487
D. Hackel	L-490
S. Haney	L-490
M. Henesian	L-490
S. Haan	L-477
J. Hunt	L-465
K. Jancaitis	L-490
J. Kilkenny	L-488
B. Krupke	L-590
L. Lawson	L-490
C. Laumann	L-487
H. Lowdermilk	L-490
J. Lindl	L-488
K. Manes	L-465
D. Milam	L-487
J. R. Murray	L-465
J. E. Murray	L-495
C. Orth	L-490
T. Parham	L-487
J. Paisner	L-488
D. Pennington	L-493
M. Perry	L-493
H. Powell	L-488
J. Rothenberg	L-439
P. Renard	L-490
R. Sacks	L-490
R. Sawicki	L-465
R. Speck	L-495
E. Storm	L-488
J. Trenholme	L-490
B. Van Wouterghem	L-476
C. Vann	L-493
P. Wegner	L-495
T. Weiland	L-479
C. Widmayer	L-443
R. Wilcox	L-490
W. Williams	L-490